IEEE Access
Multidisciplinary | Rapid Review | Open Access Journal

Received November 7, 2019, accepted November 20, 2019, date of publication November 25, 2019,
date of current version December 9, 2019.

Digital Object Identifier 10.1109/ACCESS.2019.2955564

Improving Depth Sensitive Fluorescence Spectroscopy With Wavefront Shaping by Spectral and Spatial Filtering

CHAO-MAO HSIEH, MANISH VERMA, AND QUAN LIU
School of Chemical and Biomedical Engineering, Nanyang Technological University, Singapore 637459

Corresponding author: Quan Liu (quanliu@ntu.edu.sg)

This work was supported in part by the Ministry of Education in Singapore through its Tier 2 under Grant MOE2015-T2-2-112 and Grant MOE2017-T2-2-057, in part by the Nanyang Technological University (NTU) through its NTU-AIT-MUV Programme in Advanced Biomedical Imaging under Grant NAM/15004, and in part by the Agency for Science, Technology and Research (A*STAR) through its Industry Alignment Fund (Pre-Positioning) under Grant H17/01/a0/008 and Grant H17/01/a0/0F9.

ABSTRACT Depth sensitive optical spectroscopy preferentially detects optical spectra from different depths in layered samples, which plays a crucial role in many applications such as the optical diagnosis of epithelial precancer and cancer. In depth sensitive optical measurements, multiple light scattering in tissues significantly degrades the depth sensitivity to a subsurface target layer. To address this issue, feedback based wavefront shaping led by guide stars can be used to refocus light to increase the depth sensitivity to a target layer. However, the lack of intrinsic guide stars in tissues or tissue-like samples often leads to poor enhancement in depth sensitive Raman/fluorescence measurements (∼20% in the past literature) from the target layer due to the contribution from the overlaying non-target layer. In this study, we demonstrate that spatial filtering and spectral filtering can significantly improve the performance of depth sensitive fluorescence spectroscopy assisted by feedback based wavefront shaping in tissue-like scattering phantoms. The two filtering techniques work by effectively increasing the relative contribution from the target layer to the feedback signal during wavefront optimization through spatially and spectrally rejecting off-target fluorescence light, which is essentially similar to the role of time or coherence gating. When the filtering techniques are applied, a maximum of three-fold enhancement in fluorescence contribution from the target layer is observed, which is in contrast to nearly no enhancement in case of no filtering. This significant enhancement has not been reported previously for depth sensitive optical spectroscopy in the area of feedback based wavefront shaping. Therefore, our work represents a new advance towards the application of wavefront shaping in depth resolved optical spectroscopy for the characterization of layered structures such as epithelial tissues or drug tablets, in which the creation of an external guide star is challenging or not allowed.

INDEX TERMS Depth sensitive fluorescence spectroscopy, spatial filtering, spectral filtering, feedback based wavefront shaping.

I. INTRODUCTION

Depth dependent distribution of endogenous fluorophores and other intrinsic biomolecules reveals important diagnostic information about the progress of diseases such as cancer in epithelial tissues [1] thus is critical to early diagnosis. Depth-sensitive optical spectroscopy has been proposed to detect optical spectra from different depths in such layered tissues. Early optical probes based on fiber optics for depth-sensitive optical spectroscopy [2], [3] are rugged and convenient for *in vivo* hand-held measurements but suffer from low spatial resolution due to the divergence nature of light coming out of optical fibers. Similar techniques such as spatial offset Raman spectroscopy [4], [5] have been applied to Raman spectroscopy. Meanwhile, optical probes based on an objective lens [6] were proposed to implement non-contact measurements to reduce the uncertainty in contact pressure and spectral acquisition, which also improves the spatial resolution since the light can be focused by the objective lens. However, this setup requires the movement of the objective

The associate editor coordinating the review of this manuscript and approving it for publication was Yizhang Jiang.

lens multiple times to collect optical spectra from a range of depths. To speed up depth sensitive measurements, our group proposed to use an axicon lens [7] to create a focal line covering a range of depths and detect optical spectra from all the depths in one measurement. While the above techniques for depth sensitive optical spectroscopy have made significant improvement in reducing uncertainty and speeding up measurements, the depth sensitivity that can be achieved by these techniques degrades dramatically with an increasing depth due to multiple light scattering in tissues.

Various methods have been proposed to overcome the issue of multiple light scattering in the imaging of turbid media such as tissues. Optical coherence tomography (OCT) and related techniques [8], [9] take advantage of coherence gating and can image up to 2 mm, but its principle is not applicable to fluorescence spectroscopy. Multiphoton microscopy [10] works nicely for deep tissue imaging or spectroscopy, but it requires a complicated and costly setup involving a pulsed laser thus not preferred in clinical diagnosis. Time gating [11]–[13] and spatial frequency domain imaging [14] have been demonstrated for reflectance measurements but not for fluorescence spectroscopy likely due to weak signals. Recently, wavefront shaping [15], [16] and related techniques including transmission matrix measurements, etc. References [17]–[20] have emerged as a promising technique to provide an alternative for imaging through a turbid medium and focusing light in turbid media using linear [21] or nonlinear optical techniques [22], [23]. By increasing constructive interference in a turbid sample, wavefront shaping refocuses light onto a single small spot to enhance the incident energy on the target. Note that the goal here is different from that in adaptive optics (AO), which is intended to correct aberration in a distorted image to improve imaging quality [24].

Among these techniques, feedback based wavefront shaping is known for its versatility [24], [25]. However, one well-known weakness of this technique is the requirement of a guide star. An external guide star [26] is inconvenient or sometimes even impossible in future clinical applications. Although an internal guide star utilizing non-linear optical focusing or internal absorption contrast in tissues is useful [27], [28], the relevant methods that have been reported in the literature either involve a complicated setup or are not applicable in depth sensitive optical spectroscopy. Without these special guide stars, the past study for depth sensitive Raman spectroscopy has shown only slight enhancement [29], which suggests that the enhancement for fluorescence spectroscopy would be even poorer due to potential photobleaching. To address this problem, we propose to explore two common optical techniques that have not been fully exploited in feedback based wavefront shaping to our best knowledge, i.e., spatial filtering and spectral filtering, in an attempt to increase the depth sensitivity to a subsurface target in depth sensitive fluorescence spectroscopy. The advantage of using fluorescence as the feedback signal is that it is suitable for any target with low scattering contrast. In such a case, it is difficult to use reflected excitation light as the feedback signal for light optimization since it may be too weak to detect. Moreover, the depth dependent distribution of endogenous fluorophores in some tissues such as epithelial tissues could be utilized to increase the depth sensitivity to a particular layer. Our results show that the depth sensitivity to fluorophores in the bottom layer of a two-layered tissue phantom in a reflection setup can be enhanced significantly with proper spatial filtering and spectral filtering of guiding light for wavefront optimization compared to the situation without such filtering. The filtering plays a role similar to coherence or time gating, i.e., to select the light coming from the target zone for wavefront shaping.

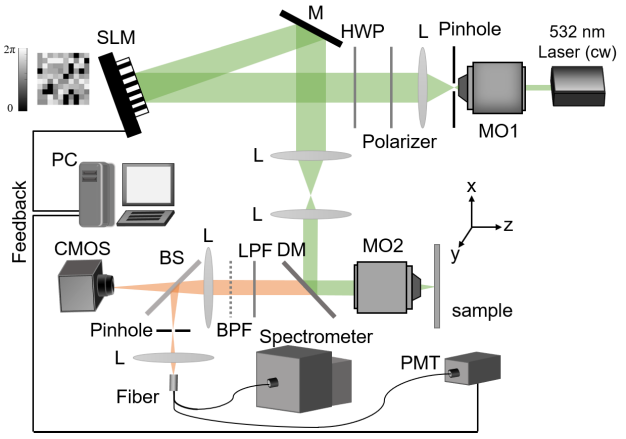

FIGURE 1. Experimental setup. M: Mirror; L: lens; HWP: half-wave plates; LPF: 532 nm long-pass filter; BPF: band-pass filter; SLM: spatial light modulator; MO1: 20× microscope objective; MO2: 50× microscope objective; BS: beam splitter; DM: 532 nm dichroic mirror; PMT: photomultiplier tube.

The current gap in this area is that the past study in depth sensitive optical spectroscopy using wavefront shaping without special guide stars showed only slight enhancement (around ∼20% increase) [29]. This is insufficient to achieve any meaningful result. Our main contribution in this study is to demonstrate that the enhancement factor using wavefront shaping for depth sensitive optical spectroscopy can be increased to about 300% with the help of spatial filtering and spectral filtering. This has not been reported previously for depth sensitive optical spectroscopy in the area of feedback based wavefront shaping. Therefore, our work represents a new advance towards the application of wavefront shaping in depth resolved optical spectroscopy. Moreover, we show that a tradeoff needs to be made on the filtering parameters because of the positive effects of spatial/spectral filtering in wavefront shaping performance and the decreasing signal-to-noise ratio associated with filtering.

II. MATERIALS AND METHODS

A. EXPERIMENTAL SETUP

The schematic of the experimental setup is shown in Figure 1. Continuous-wave coherent laser light (Millennia eV 5W, Spectra-Physics, Santa Clara, California, USA) is cleared up by passing through a spatial filter, which is then projected

onto a Spatial Light Modulator (SLM, PLUTO-2-VIS, HOLOEYE, Berlin, Germany) with a resolution of 1920 × 1080 pixels. A half-wave plate and a linear polarizer are used to adjust the power and polarization to match the requirement of the SLM. The light is expanded to fill the SLM as much as possible for optimal modulation. The modulated light is demagnified first and then focused onto the sample by a 50× microscope objective (UMPlan FI; Olympus, Shinjuku, Tokyo, Japan) with an NA of 0.8 and a working distance (WD) of 0.6 mm. The fluorescence light excited from the sample is collected by the same microscope objective. The sample is mounted on a three-dimensional stage (PT3/M; Thorlabs, Newton, New Jersey, USA) for precise adjustment. Emitted fluorescence is separated from the excitation light by a long-pass dichroic mirror (DM; Di03-R532; Semrock, Rochester, New York, USA). A long-pass filter (BLP01-532R-25; Semrock, Rochester, New York, USA) afterwards further attenuates the excitation light. When the effect of spectral filtering on wavefront shaping is evaluated, none or one of the two band-pass filters (FF01-618/50; FF01-650/60; Semrock, Rochester, New York, USA) is placed right behind the long-pass filter to select the desired spectral band of fluorescence.

A photomultiplier tube (PMT, 77348, Newport Corporation, California, USA) driven by a high voltage power supply (70705, Spectra-physics, Santa Clara, California, USA) and preceded by a preamplifier (SR560; Stanford research systems, Sunnyvale, CA, USA) is used to detect fluorescence for SLM optimization. When the effect of spatial filtering is evaluated, several pinholes with a range of diameters (P800H, P200H, P150H, P100H and P75H, Thorlabs, Newton, New Jersey, USA) are placed on the image plane one at a time to prevent unwanted light from being captured by the PMT or spectrometer. Once the optimization is complete, the spectrum will be recorded by a PI spectrometer that consists of a spectrograph (Acton SP2150; Princeton Instruments, Trenton, New Jersey, USA) and a CCD camera (PIXIS 400; Princeton Instruments, Trenton, New Jersey, USA). To increase light collection efficiency after the pinhole, a condenser with a magnification of 0.5 is placed before a round-to-linear fiber bundle (BFL105HS02, Thorlabs, Newton, New Jersey, USA) with an effective core diameter of 355 μm on the round end, and the size of the linear end matches the input slit width of the spectrometer.

B. PHANTOM PREPARATION

Scattering tissue phantoms were made by mixing titanium dioxide (TiO_2 of 1.5 μm; US Research Nanomaterials Inc., Houston, USA) in dissolved polydimethylsiloxane (PDMS, Sylgard 184; Dow Corning, Midland, Michigan, USA) [30]. The reduced scattering coefficient (μ_s') was adjusted by varying the concentration of TiO_2 in PDMS according to the calculation using Mie theory with known refractive index, particle size, and volume fraction [31]. Purple fluorescent microparticles (FH-2062-2; Spherotech, Libertyville, IL, USA) and Rhodamine 6G (R6G 56226; Sigma-Aldrich, St. Louis, MO, USA) were separately suspended in isopropyl alcohol (IPA W292907; Sigma-Aldrich, St. Louis, MO, USA) first, then were added into different TiO_2 phantoms in PDMS before setting. Every sample was continuously stirred on a magnetic stirring hot plate for at least 1 hour to ensure the homogeneous distribution of particles or R6G in PDMS. The concentration of the particles was adjusted to around 3×10^7 particles/g in PDMS, and the concentration of R6G was 128 μM in PDMS. Then each sample was mixed with a curing agent so that PDMS set to form a solid phantom. A two-layered sample was made by stacking one layer with R6G on top of the other with the fluorescence microparticles. The transport mean free path ($l_t = 1/\mu_s$') of the top layer was around 3.3 mm with a thickness of 110 ± 10 μm, to mimic the epithelium in epithelial tissue [32]. The transport mean free path of the bottom layer was around 10 mm with a thickness from 110 ± 10 μm to serve as the superficial region of the stroma.

C. SLM MODULATION

The continuous sequential algorithm [33] was used to update the phase values of the SLM in the study. A total of 1,000 × 1,000 pixels on the SLM were binned into 10 × 10 grids, i.e. 100 × 100 pixels in each grid. The phase shift from 0 to 2π with an increment of 0.2π was utilized during optimization with a total of 1,000 iterations in each experiment. Briefly, the algorithm is to optimize the feedback signal by modulating phase for each grid in the spatial light modulator individually. In the iteration process, the feedback signal will be measured with a different phase for each grid in a range of 0 to 2π. After the measurements, the phase of the segment will be set to the value that yields the maximum feedback signal. The process will continue for each grid until the phase values of all grids are set. Due to its high sensitivity, a PMT was used to collect fluorescence during wavefront optimization. The PMT reading served as a feedback signal in each iteration for wavefront optimization so that it would be maximized at the end of wavefront shaping. The fluorescence spectrum was measured using a commercial spectrometer after the wavefront was optimized.

D. ENHANCEMENT FACTOR AND EMISSION RATIO

The fluorescence spectra of pure R6G and purple fluorescent particles at low concentrations are shown in Fig. 2B. The spectral contribution from each fluorophore is estimated by curve fitting, in which a spectrum measured from a two-layered sample (Fig. 2A) is modeled as the summation of the spectral contributions from pure R6G and fluorescent particles each linearly related to the respective concentration. The spectrum contributed by each fluorophore is integrated from 540 nm to 670 nm to estimate the fluorescence contribution for the calculation of the enhancement factor and emission ratio.

The enhancement factor is defined as the ratio of fluorescence contribution from the purple fluorescence particles

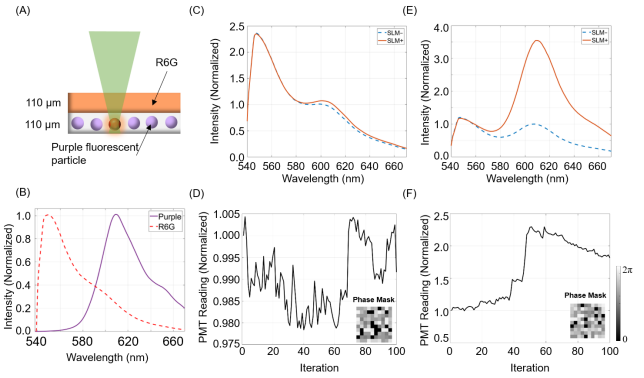

FIGURE 2. Enhancement of emitted fluorescence with and without a 200-μm pinhole. (A) Schematic of the two-layered sample with R6G in the top layer and purple fluorescent particles in the bottom layer. (B) Individual fluorescence spectra of R6G and purple fluorescent microparticles. (C) & (E) fluorescence spectra before (blue dash line with the legend "SLM–") and after (orange solid line with the legend "SLM+") wavefront optimization detected (C) without and (E) with a 200-μm pinhole, respectively. The spectra have been normalized by dividing each spectrum by the purple fluorescent peak before wavefront optimization to facilitate enhancement visualization. (D) & (F) PMT reading during optimization and the resulting phase mask at the end obtained (D) without and (F) with a 200-μm pinhole, respectively. Only a long-pass filter was used to remove excitation light and there was no band-pass filter involved.

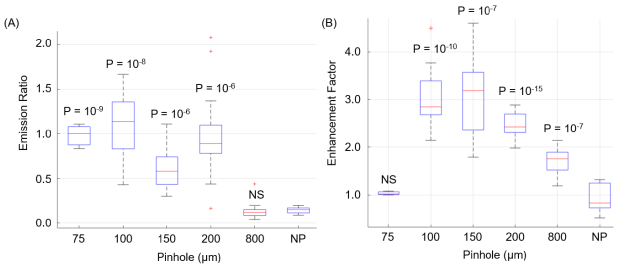

FIGURE 3. Effect of spatial filtering using pinholes on the performance of wavefront optimization. (A) Emission ratio as a function of pinhole diameter. (B) Enhancement factor as a function of pinhole diameter. Only a long-pass filter is used to obtain the data. The p-value is calculated from the two-sided t-test on the difference between each experimental group with a different pinhole diameter and the controlled group with no pinhole. NS: Not significant. NP: No pinhole.

after wavefront optimization to that before optimization [34] both after background subtraction.

For a two-layered sample with a different fluorophore in each layer, the emission ratio, defined as the ratio of fluorescence contribution from purple fluorescent particles to the fluorescence contribution from R6G, is used to quantify the sensitivity of the collected signal to the bottom layer.

E. SPECTRAL AND SPATIAL FILTERING

The effect of spatial filtering on the performance of wavefront optimization is evaluated for a series of pinholes with a range of diameters, including 800 μm, 200 μm, 150 μm, 100 μm, and 75 μm. The pinhole is mounted at the conjugate position of the presumed target spot in the sample. Its size controls the amount of fluorescence light detected from the target spot. A smaller pinhole can reject off-target light more efficiently. However, the detected signal will be also weaker, which will reduce the signal-to-noise ratio. Therefore, a tradeoff needs to be made between the spatial filtering effect and signal-to-noise ratio.

When investigating the effect of spectral filtering, a filter holder is placed immediately after the 532-nm long-pass filter as shown in Fig. 1. The enhancement factor is determined with an empty holder first, which serves as the control experiment. Then the holder is loaded with two band-pass filters, i.e., 618 $\pm$ 25 nm and 650 $\pm$ 30 nm, sequentially and the enhancement factor is determined again. Note that the passband of the first filter matches the fluorescence peak of the purple fluorescent particles while that of the second filter matches the sideband of the purple fluorescent particles. As the passband red shifts from one filter to the other, the relative fluorescence contribution from the bottom layer increases thus should promote the performance of wavefront shaping for depth sensitive measurements from the bottom layer. However, the overall fluorescence intensity would decrease in this case resulting in lower signal-to-noise ratio. Therefore, a tradeoff needs to be made between the spectral filtering effect and signal-to-noise ratio, which is similar to spatial filtering.

III. EXPERIMENTAL RESULTS

To facilitate the observation of fluorescence from each layer, a two-layered phantom sample is used in this study as shown in Fig. 2(A). Fig. 2(B) shows the individual fluorescence spectra of two fluorophores used, i.e. R6G and purple fluorescent microparticles. Without a pinhole, it can be seen in Fig. 2(C) that the enhancement factor is quite low (around 110%) after wavefront optimization. Moreover, the PMT reading appears random in this case as shown in Fig. 2(D) during optimization. After a 200-μm pinhole is placed in the position conjugate to the supposed focus in the sample to reject out-of-focus light, a much greater enhancement factor (around 350%) is observed as shown in Fig. 2(E). Moreover, the PMT Reading goes up steadily as shown in Fig. 2(F) by 50 iterations. After that, the photobleaching starts to take over, and the PMT reading goes down.

The effect of spatial filtering on the performance of wavefront optimization is evaluated for a series of pinhole diameters, including 800 μm, 200 μm, 150 μm, 100 μm, and 75 μm, as shown in Fig. 3. Note that the image of each individual particle is around 105 μm on the pinhole plane according to that taken by the camera located on the conjugate position. Fig. 3(A) shows that the contribution from the bottom layer significantly increases when the pinhole diameter decreases from 800 μm to 200 μm or a smaller value, which implies the effectiveness of spatial filtering using a pinhole with a diameter of 200 μm or smaller to reject out-of-focus light for subsequent wavefront optimization. Fig. 3(B) shows that the enhancement factor increases first as the pinhole size decreases and reaches the maximum at a pinhole diameter of 150 μm. After that, the enhancement factor

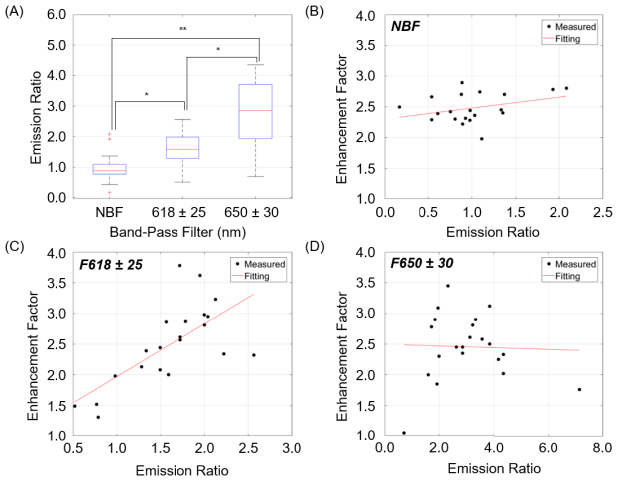

FIGURE 4. Effect of spectral filtering using band-pass filters on the performance of wavefront optimization. (A) Emission ratio as a function of the central wavelength of the band-pass filter. Enhancement factor as a function of the emission ratio in the cases of (B) no band-pass filter, (C) with a band-pass filter 618 ± 25 nm (D) with a band-pass filter 650 ± 30 nm. A 200-μm pinhole is used to obtain these data. The p-value in (A) is calculated from the two-sided t-test on the difference in emission ratio between each pair of groups. NBF: No Band-pass Filter. **P<10^{-9}; *P<10^{-5}.

appears to decrease until there is no enhancement at a pinhole diameter of 75 μm. It is noted that the maximum enhancement is achieved at a pinhole diameter of around 150 μm that roughly matches the particle image size on the pinhole plane.

The effect of spectral filtering on the performance of wavefront optimization is evaluated in the cases of without a band-pass filter and with a band-pass filter as shown in Fig. 4. Since the fluorescence peaks of the two-layer sample is around 550 nm (R6G in the top layer) and 610 nm (purple-color fluorescent particles in the bottom layer) respectively, spectral filtering with a band-pass filter of 650 ± 30 nm or 618 ± 25 nm increases the fluorescence contribution from the bottom layer as shown in Fig. 4(A). Fig. 4(C) shows a clear monotonic relation between the enhancement factor and emission ratio when using the band-pass filter 618 ± 25 nm, which demonstrates the positive effect of spectral filtering on the performance of wavefront optimization. In contrast, such a trend is unclear in the cases of without any band-pass filter and with the band-pass filter 650 ± 30 nm as shown in Fig. 4(B) and 4(D). It is not surprising to see an unclear increasing trend in enhancement factor in Fig. 4(B) because fluorescence for guiding wavefront optimization can come from both layers without any band-pass filter. It is also worth noting in Fig. 4(D) that, when using a 650 ± 30 nm band-pass filter, the enhancement factor seems more random than the other two cases. This can be most likely attributed to the relatively low signal-to-noise ratio in this case because the passband of this filter covers only the tail region of the fluorescence peak in the bottom layer. Consequently, the enhancement factor is influenced as discussed in the discussion section.

IV. DISCUSSION

Spatial and spectral filtering can effectively improve the enhancement factor as illustrated in Fig. 2 & 3 and Fig. 4, respectively. The positive role of spatial and spectral filtering in feedback based wavefront shaping can be attributed to the fact that both filtering techniques increase the relative contribution from the target layer to the feedback signal during wavefront optimization by spatially and spectrally rejecting off-target fluorescence light, which is similar to the roles of the pinhole and bandpass filter in confocal fluorescence microscopy. Spatial filtering with a pinhole works as long as the target depth is not too large and the guiding light is still detectable, usually within a few scattering mean free paths [35]. Spectral filtering can work for depth sensitive fluorescence spectroscopy in epithelial tissue since it is well known that endogenous fluorophores in the epithelium and stroma of epithelial tissues are different with distinctive peaks [36]. To apply these techniques in a real tissue requires that feedback based wavefront shaping is faster than speckle decorrelation in tissues [37], [38], which is currently an active field of research.

Another critical factor in optimization is the signal-to-noise ratio (SNR) of the feedback signal. Since the optimization relies on whether the feedback signal increases or decreases with the change in wavefronts, it is important for the feedback signal to possess a reasonable SNR for stable optimization. If the SNR is too small, the optimization may not be as effective, which is demonstrated in Fig. 3 and Fig. 4(D). In Fig. 3, the increasing trend in enhancement factor with a decrease in pinhole size changes when the pinhole is smaller than 150 μm, and there is nearly no enhancement for a pinhole size of 75 μm, which can be explained by the poor SNR in these cases. Similarly, the increasing trend in enhancement factor with an increase in emission ratio as shown in Fig. 4(D) is supposed to be more significant than that in Fig. 4(C) if only considering that a greater portion of detected fluorescence light comes from the target layer with the filter F650 ± 30 compared with the other filter F618 ± 25. However, this trend is not seen most likely due to the poor SNR of the feedback signal as the filter F650 ± 30 can only catch the weak tail of the fluorescence peak from the target fluorophore. This SNR issue can be much more serious in biological tissues from which the endogenous fluorescence signal is weaker than phantoms samples or exogenous contrast agents. This suggests that using a pulsed laser as the excitation source to achieve a better SNR in the feedback signal may be desirable in future tissue measurements to achieve greater enhancement and faster optimization.

One issue encountered in this study and also common in fluorescence spectroscopy is the photobleaching of fluorophores, which makes it difficult to reach the maximum enhancement [15]. In this study, the photobleaching rate is estimated by monitoring the emitted fluorescence of an individual particle over time with a range of incident powers. A laser power of around 10 to 40 μW is found yielding minimal

photobleaching and decent SNR thus used during wavefront optimization. With such an incident power, the emitted fluorescence drops only moderately during optimization, and the fluorescence intensity is high enough to be measured even by an sCMOS camera for successful optimization. However, it is anticipated that photobleaching may become increasingly severe as the ongoing optimization tends to increase the laser power density on the target particle. One possible solution for reducing photobleaching is to dynamically adjust the laser power during optimization. Higher laser power can be used in the initial period of wavefront optimization to achieve enhancement before severe photobleaching occurs. Then the laser power can be reduced to slow down photobleaching but is still high enough to yield detectable fluorescence. The fluorescence reading can be numerically scaled up to compensate for its drop due to the laser power reduction. Certainly, using a pulsed laser source could be another solution as mentioned earlier.

Although the continuous sequential algorithm takes a longer time than several other algorithms such as the optimal steepest ascent algorithm, it has certain advantages and is suitable in this study. First, the continuous increase in intensity can improve the signal-to-noise ratio for proper signal enhancement with a weak feedback signal. Second, compared to the faster optimal steepest ascent algorithm method we evaluated, the continuous sequential algorithm can achieve a higher signal enhancement factor at the end. For a static sample such as the one used in the study with a long speckle decorrelation time [38], the continuous sequential algorithm is a proper choice.

One significant difference between phantom samples here (as well in most other papers about wavefront shaping) and real tissue samples is the distribution of fluorophores. While the distribution of endogenous fluorophores in tissues such as NADH (reduced nicotinamide adenine dinucleotide) and FAD (flavin adenine dinucleotide) [39] is relatively dense and continuous in cells, the target purple fluorescence particles in this study are discrete and sparse. The discrete and sparse distribution of the target fluorescence particles with adequate distance between any pair of them artificially reduces the sample volume contributing to the feedback signal and improves the enhancement. This implies that the enhancement can be worse in real tissue samples because the sample volume contributing to the feedback signal can be much larger due to the proximity of surrounding fluorophore molecules. In fact, we did evaluate a phantom sample with dissolved Rhodamine 6G (R6G) as the fluorophore in PDMS and could not achieve any significant enhancement even with pinholes. The distribution of R6G in this sample is continuous since R6G is well dissolved before PDMS setting. It is anticipated that one should be able to observe fluorescence enhancement in this case when the pinhole size is sufficiently small; however, the challenge lies in providing the feedback fluorescence signal with a sufficient SNR. This could be achieved with a system equipped with a pulsed laser and a sensitive detector.

The long-term goal of this study is to apply wavefront shaping to tissue imaging. The heterogeneous structure of an actual tissue could be imaged by sequentially scanning the target spot, which is conjugate to the pinhole, throughout the tissue. During scanning, the size of the pinhole can be varied to achieve the tradeoff between the spatial resolution and the signal-to-noise ratio. The spectral filter can be also switched to match various target fluorophores. Some weaknesses of the current technique that need to be addressed before that include the slow speed and low sensitivity. While the former weakness prevents wavefront shaping from being applied in a real tissue with a short speckle decorrelation time, the latter weakness limits the maximum imaging depth. We are currently working on these two weaknesses by modulating the signal out of the target spot to suppress that from the surrounding region, which could bring this technique closer to real tissue imaging.

V. CONCLUSION

We demonstrate that spatial filtering and spectral filtering can significantly improve the performance of depth sensitive fluorescence spectroscopy assisted by feedback based wavefront shaping in tissue-like scattering phantoms. The two filtering techniques work by effectively increasing the relative contribution from the target layer to the feedback signal during wavefront optimization through spatially and spectrally rejecting off-target fluorescence light, which is substantially similar to the role of time or coherence gating. When the filtering techniques are applied, a maximum of three-fold enhancement factor in fluorescence contribution from the target layer is observed, which is in contrast to nearly no enhancement in case of no filtering. These two techniques integrated with feedback based wavefront shaping can improve depth sensitive fluorescence spectroscopy for the characterization of layered structures such as epithelial tissues or tablets, in which the creation of an external guide star is challenging or not allowed.

REFERENCES

[1] I. Pavlova, K. Okolov, R. Drezek, A. Malpica, M. Follen, and R. Kortum, "Microanatomical and biochemical origins of normal and precancerous cervical autofluorescence using laser-scanning fluorescence confocal microscopy," *Photochem. Photobiol.*, vol. 77, no. 5, pp. 550–555, 2003.

[2] Q. Liu and N. Ramanujam, "Experimental proof of the feasibility of using an angled fiber-optic probe for depth-sensitive fluorescence spectroscopy of turbid media," *Opt. Lett.*, vol. 29, no. 17, pp. 2034–2036, 2004.

[3] Q. Liu and N. Ramanujam, "Sequential estimation of optical properties of a two-layered epithelial tissue model from depth-resolved ultraviolet–visible diffuse reflectance spectra," *Appl. Opt.*, vol. 45, no. 19, pp. 4776–4790, 2006.

[4] A. Mahadevan-Jansen, M. F. Mitchell, N. Ramanujam, U. Utzinger, and R. Richards-Kortum, "Development of a fiber optic probe to measure NIR Raman spectra of cervical tissue *in vivo*," *Photochem. Photobiol.*, vol. 68, no. 3, pp. 427–431, 1998.

[5] P. Matousek, "Deep non-invasive Raman spectroscopy of living tissue and powders," *Chem. Soc. Rev.*, vol. 36, no. 8, pp. 1292–1304, 2007.

[6] S. F. Bish, N. Rajaram, B. S. Nichols, and J. W. Tunnell, "Development of a noncontact diffuse optical spectroscopy probe for measuring tissue optical properties," *J. Biomed. Opt.*, vol. 16, no. 12, 2011, Art. no. 120505.

[7] Y. H. Ong and Q. Liu, "Axicon lens-based cone shell configuration for depth-sensitive fluorescence measurements in turbid media," *Opt. Lett.*, vol. 38, no. 15, pp. 2647–2649, 2013.

[8] U. Morgner, W. Drexler, F. X. Kärtner, X. D. Li, C. Pitris, E. P. Ippen, and J. G. Fujimoto, "Spectroscopic optical coherence tomography," *Opt. Lett.*, vol. 25, no. 2, pp. 111–113, 2000.
[9] C. Dunsby and P. M. W. French, "Techniques for depth-resolved imaging through turbid media including coherence-gated imaging," *J. Phys. D, Appl. Phys.*, vol. 36, no. 14, p. R207, 2003.
[10] F. Helmchen and W. Denk, "Deep tissue two-photon microscopy," *Nature Methods*, vol. 2, pp. 932–940, Nov. 2005.
[11] S. Kang, S. Jeong, W. Choi, H. Ko, T. D. Yang, J. H. Joo, J.-S. Lee, Y.-S. Lim, Q.-H. Park, and W. Choi, "Imaging deep within a scattering medium using collective accumulation of single-scattered waves," *Nature Photon.*, vol. 9, pp. 253–258, Mar. 2015.
[12] Se. Jeong, Y.-R. Lee, W. Choi, S. Kang, J. H. Hong, J.-S. Park, Y.-S. Lim, H.-G. Park, and W. Choi, "Focusing of light energy inside a scattering medium by controlling the time-gated multiple light scattering," *Nature Photon.*, vol. 12, no. 5, pp. 277–283, 2018.
[13] M. Kadobianskyi, I. N. Papadopoulos, T. Chaigne, R. Horstmeyer, and B. Judkewitz, "Scattering correlations of time-gated light," *Optica*, vol. 5, no. 4, pp. 389–394, 2018.
[14] R. B. Saager, A. N. Dang, S. S. Huang, K. M. Kelly, and A. J. Durkin, "Portable (handheld) clinical device for quantitative spectroscopy of skin, utilizing spatial frequency domain reflectance techniques," *Rev. Sci. Instrum.*, vol. 88, no. 9, 2017, Art. no. 094302.
[15] I. M. Vellekoop, E. G. van Putten, A. Lagendijk, and A. P. Mosk, "Demixing light paths inside disordered metamaterials," *Opt. Express*, vol. 16, no. 1, pp. 67–80, 2008.
[16] A. P. Mosk, A. Lagendijk, G. Lerosey, and M. Fink, "Controlling waves in space and time for imaging and focusing in complex media," *Nature Photon.*, vol. 6, pp. 283–292, May 2012.
[17] Y. Choi, T. D. Yang, C. Fang-Yen, P. Kang, K. J. Lee, R. R. Dasari, M. S. Feld, and W. Choi, "Overcoming the diffraction limit using multiple light scattering in a highly disordered medium," *Phys. Rev. Lett.*, vol. 107, no. 2, 2011, Art. no. 023902.
[18] J. Bertolotti, E. G. van Putten, C. Blum, A. Lagendijk, W. L. Vos, and A. P. Mosk, "Non-invasive imaging through opaque scattering layers," *Nature*, vol. 491, pp. 232–234, Nov. 2012.
[19] M. Kim, W. Choi, Y. Choi, C. Yoon, and W. Choi, "Transmission matrix of a scattering medium and its applications in biophotonics," *Opt. Express*, vol. 23, no. 10, pp. 12648–12668, 2015.
[20] I. N. Papadopoulos, J.-S. Jouhanneau, J. F. A. Poulet, and B. Judkewitz, "Scattering compensation by focus scanning holographic aberration probing (F-SHARP)," *Nature Photon.*, vol. 11, pp. 116–123, Dec. 2016.
[21] I. M. Vellekoop and C. M. Aegerter, "Scattered light fluorescence microscopy: Imaging through turbid layers," *Opt. Lett.*, vol. 35, no. 8, pp. 1245–1247, 2010.
[22] O. Katz, E. Small, Y. Guan, and Y. Silberberg, "Noninvasive nonlinear focusing and imaging through strongly scattering turbid layers," *Optica*, vol. 1, no. 3, pp. 170–174, 2014.
[23] J. V. Thompson, B. H. Hokr, G. A. Throckmorton, D. Wang, M. O. Scully, and V. V. Yakovlev, "Enhanced second harmonic generation efficiency via wavefront shaping," *ACS Photon.*, vol. 4, no. 7, pp. 1790–1796, 2017.
[24] R. Horstmeyer, H. Ruan, and C. Yang, "Guidestar-assisted wavefront-shaping methods for focusing light into biological tissue," *Nature Photon.*, vol. 9, pp. 563–571, Aug. 2015.
[25] I. M. Vellekoop, "Feedback-based wavefront shaping," *Opt. Express*, vol. 23, no. 9, pp. 12189–12206, 2015.
[26] H. Ruan, T. Haber, Y. Liu, J. Brake, J. Kim, J. M. Berlin, and C. Yang, "Focusing light inside scattering media with magnetic-particle-guided wavefront shaping," *Optica*, vol. 4, no. 11, pp. 1337–1343, 2017.
[27] J. Tang, R. N. Germain, and M. Cui, "Superpenetration optical microscopy by iterative multiphoton adaptive compensation technique," *Proc. Nat. Acad. Sci. USA*, vol. 109, no. 22, pp. 8434–8439, 2012.
[28] P. Lai, L. Wang, J. W. Tay, and L. V. Wan, "Photoacoustically guided wavefront shaping for enhanced optical focusing in scattering media," *Nature Photon.*, vol. 9, pp. 126–132, Jan. 2015.
[29] J. V. Thompson, G. A. Throckmorton, B. H. Hokr, and V. V. Yakovlev, "Wavefront shaping enhanced Raman scattering in a turbid medium," *Opt. Lett.*, vol. 41, no. 8, pp. 1769–1772, 2016.
[30] G. J. Greening, R. Istfan, L. M. Higgins, K. Balachandran, D. M. Roblyer, M. C. Pierce, and T. J. Muldoon, "Characterization of thin poly(dimethylsiloxane)-based tissue-simulating phantoms with tunable reduced scattering and absorption coefficients at visible and near-infrared wavelengths," *J. Biomed. Opt.*, vol. 19, no. 11, 2014, Art. no. 115002.
[31] C. Mätzler, "MATLAB functions for Mie scattering and absorption, version 2," Inst. Angew. Phys., Univ. Bern, Bern, Switzerland, IAP Res. Rep. 2002-11, 2002, vol. 8, no. 1.
[32] C. Zhu and Q. Liu, "Validity of the semi-infinite tumor model in diffuse reflectance spectroscopy for epithelial cancer diagnosis: A Monte Carlo study," *Opt. Express*, vol. 19, no. 18, pp. 17799–17812, 2011.
[33] I. M. Vellekoop and A. Mosk, "Phase control algorithms for focusing light through turbid media," *Opt. Commun.*, vol. 281, no. 11, pp. 3071–3080, Jun. 2008.
[34] B. Blochet, L. Bourdieu, and S. Gigan, "Focusing light through dynamical samples using fast continuous wavefront optimization," *Opt. Lett.*, vol. 42, no. 23, pp. 4994–4997, 2017.
[35] S. B. Purnapatra, S. Bera, and P. P. Mondal, "Spatial filter based Bessel-like beam for improved penetration depth imaging in fluorescence microscopy," *Sci. Rep.*, vol. 2, Sep. 2012, Art. no. 692.
[36] N. Ramanujam, "Fluorescence spectroscopy of neoplastic and non-neoplastic tissues," *Neoplasia*, vol. 2, nos. 1–2, pp. 89–117, 2000.
[37] M. Nixon, O. Katz, E. Small, Y. Bromberg, A. A. Friesem, Y. Silberberg, and N. Davidson, "Real-time wavefront shaping through scattering media by all-optical feedback," *Nature Photon.*, vol. 7, pp. 919–924, Oct. 2013.
[38] Y. Liu, P. Lai, C. Ma, X. Xu, A. A. Grabar, and L. V. Wang, "Optical focusing deep inside dynamic scattering media with near-infrared time-reversed ultrasonically encoded (TRUE) light," *Nature Commun.*, vol. 6, Jan. 2015, Art. no. 5904.
[39] N. Ramanujam, "Fluorescence spectroscopy *in vivo*," *Encyclopedia Anal. Chem.*, vol. 1, pp. 20–56, Sep. 2000.

CHAO-MAO HSIEH received the bachelor's degree in life science from National Yang-Ming University, Taiwan, the master's degree in biomedical electronics and bioinformatics from the National Taiwan University, Taiwan. He is currently pursuing the Ph.D. degree with the School of Chemical and Biomedical Engineering, Nanyang Technological University, Singapore.

MANISH VERMA received the bachelor's and master's degrees in physics from Kurukshetra University, India, and the Ph.D. degree in physics from the Indian Institute of Technology Delhi, India. He has been a Postdoctoral Researcher with the School of Chemical and Biomedical Engineering, Nanyang Technological University, Singapore. He is currently a Postdoctoral Researcher with the Medical Optics Group, ICFO-The Institute of Photonic Science, Spain. His research is focused on development of compact and low-cost blood flow monitoring devices based on diffused optics. His research interests include diffuse optics, instrumentation, optical singularities, wavefront shaping, and coherent backscattering. He has a number of publications in many optics journals and also served as a reviewer for them.

QUAN LIU received the bachelor's degree in electrical engineering from Xidian University, Xi'an, China, the master's degree in electrical engineering from the Graduate School, University of Science and Technology of China, Beijing, China, and the Ph.D. degree in biomedical engineering from the University of Wisconsin–Madison, Madison, WI, USA. He is currently an Associate Professor with the School of Chemical and Biomedical Engineering, Nanyang Technological University, Singapore. He has published more than 60 journal articles and held nineteen patents/patent applications in the field of biomedical optics. His research interest is focused on multispectral imaging and optical spectroscopy for medical diagnostics. He is a Senior Member of SPIE. He has served as a Reviewer for several optics journals and multiple international funding agencies as well as a Committee Member and the Session Chair for multiple international conferences, such as European Conferences in Biomedical Optics (ECBO) and Photonics West BIOS.